

# Strangeness Chemical Equilibration in QGP at RHIC and LHC

Jean Letessier

*Laboratoire de Physique Théorique et Hautes Energies  
Université Paris 7, 2 place Jussieu, F-75251 Cedex 05*

Johann Rafelski

*Department of Physics, University of Arizona, Tucson, Arizona, 85721, USA*

(Dated: February 14, 2006)

We study the process of chemical equilibration of strangeness in dynamically evolving QGP fireball formed in relativistic heavy ion collisions at RHIC and LHC. We account for the contribution of direct and explore the thermal-QCD strangeness production mechanisms. The specific yield of strangeness per entropy is the primary target variable. We explore the effect of collision impact parameter, *i.e.*, fireball size, on strangeness chemical equilibration in QGP. Insights gained in study the RHIC data are applied to the study strangeness production at the LHC. We further consider how characteristic hadronic observables are influenced by the differences in the chemical equilibration, given a specific per entropy strangeness yield.

PACS numbers: 25.75.Nq, 25.75.-q, 24.10.Pa, 12.38.Mh

## I. INTRODUCTION

Conversion of kinetic collision energy into high multiplicity of newly made hadronic particles is one of the most notable features of reactions observed at the Relativistic Heavy Ion Collider (RHIC) at the Brookhaven National Laboratory (BNL) [1]. In this process, aside of light  $u$  and  $d$  quark pairs present in all matter surrounding us, the strange flavor quark pairs  $s, \bar{s}$  are produced copiously (in general in what follows the particle symbol will refer to the corresponding particle yield). The final  $s$ -yield depends on the initial reactions, and on the history of the fireball, and thus also on the nature and properties of the phase of matter formed. On the time scale of hadronic interactions, strangeness flavor is conserved, and thus prior to any weak interaction decays, we have  $\bar{s} = s$  — when we refer to strangeness yield, production, etc, we thus always address yield, production, etc, of strange quark pairs.

This study is addressing strangeness under the physical conditions achieved, at RHIC, at the highest attainable reaction energy today,  $\sqrt{s_{NN}} = 200$  GeV. We are particularly interested in the sensitivity of strangeness production to the nature and properties of the matter formed in the heavy ion reactions. Theoretical studies have shown that strangeness is produced rapidly in collisions (fusion) of thermalized gluons [2, 3], within the deconfined state, the quark-gluon plasma (QGP) formed in the central collisions of heavy nuclei. On the scale of RHIC reaction time  $\tau < 10$  fm, the hadron based reactions were found to be too slow to allow copious strangeness production after thermalization of matter and are even more ineffective to produce multi-strange hadrons [4].

On the other hand, the situation is quite different if the deconfined QGP state breaks up in a fast hadronization process: the enhancement of strange hadrons and most specifically strange antibaryons, growing with valance strange quark content of hadrons produced is the pre-

dicted characteristic property of the deconfined QGP phase [5]. This is the cases since in the breakup of the strangeness rich deconfined state, *i.e.*, hadronization, several strange quarks formed in prior, and independent, reactions can combine into a multistrange hadron.

We explore, in depth, the centrality dependence in a wide range between peripheral, and most central reactions, in which up to 90% of projectile and target nucleons participate. As the centrality of the nuclear reaction and the number of participants  $A$  decrease, the collective ‘thermal’ mechanism, and with it the strangeness enhancement effect, diminishes gradually [3]. This decrease drives a gradual decrease in the centrality dependent production rate of multistrange hadrons.

This feature is an important phenomenological marker of the kinetic particle collisions mechanism of strangeness enhancement. It differs from models obtaining the enhancement as a result of an always prevailing hadronic phase chemical equilibrium [6, 7], combined with the canonical phase space yields [8], prevailing in the N-N reference systems [9]. In this ‘canonical model’ case, the enhancement decrease is occurring suddenly at a relatively small reaction volume. As we shall show, the kinetic approach implies an enhancement increasing slowly with reaction volume and with reaction energy. The energy dependence is opposite to the prediction of the canonical mechanism, which is strongly energy dependent and increases with decreasing energy [10].

Our main objective is to understand the mechanisms of thermal strangeness production during the expansion phase of the quark-gluon fireball. Therefore, we formulate the kinetic equations allowing to address, in detail, the growth in specific strangeness per entropy  $s/S$  in the thermal QGP processes in a both, longitudinally and transversely expanding QGP fireball. We believe that strangeness chemical equilibration is subject to relatively slow reaction mechanisms as compared to chemical equilibration of the light  $q = u, d$  quarks and  $g$  gluons. These

particle can be produced by entirely soft processes which are intrinsically non-perturbative [11]. Their chemical equilibration can be further driven by multi-particle collisions [12, 13]. Therefore, we will assume relatively short relaxation times for  $q, g$  rather than to compute these using the same perturbative method as will be developed to evaluate strangeness equilibration. It is the finite strangeness mass and the measured strength of the running QCD coupling constant  $\alpha_s$  which allows us the use of perturbative formalism in study of strangeness production [14].

The chemical relaxation times for the strangeness approach to chemical equilibrium in an expanding QGP has been considered several times before [15, 16, 17, 18, 19]. Aside of the comprehensive exploration of the impact parameter dependence, and consideration of energy dependence, we further offer here several new theoretical insights. We evolve in time not the strangeness itself, but the specific strangeness per entropy  $s/S$ . In this way, we can identify more clearly the production processes of strangeness, since entropy is produced earlier on and is (nearly) conserved during the time period of thermal strangeness production.

Moreover, this quantity  $s/S$  is an experimental observable preserved in the hadronization process. Thus, we can connect the final state of the evolution directly to experimental soft hadron yield experimental results. Moreover, the selection of the initial value of  $s/S$  is much less model dependent. We find that much of the variability about the initial conditions, such as dependence on initial temperature, cancels in the final result, and thus this specific observable will be shown to yield nearly model independent insights about thermal strangeness production in QGP.

In the following section II, we begin with a brief discussion of general features relevant in all considerations presented. In subsection II D, we formulate the kinetic equations describing the growth in specific strangeness per entropy  $s/S$  and show that, at RHIC, the observed specific per entropy strangeness yield suggests that the ‘direct’ and ‘thermal’ processes are of comparable strength in most central reactions. In order to integrate as function of reaction time the strangeness yield equations, we develop a simple expansion model of the plasma phase in subsection II E.

In section III, we study the thermal strangeness production processes. We then obtain reference yields for two different expansion geometries at RHIC in subsection III A. We extrapolate this to the LHC environment in subsection III B. We explore how ‘deep’ into the early history of the hot and dense fireball the strangeness signature of thermal QGP is allowing us to look, *i.e.*, the dependence on initial conditions, in subsection III C. We then explore the influence of fundamental uncertainties, such as the present day limited knowledge about the strange quark mass and the QCD thermal effects on the freezing of the strange quark degrees of freedom, in subsection III D.

In section IV, we connect the results we obtained to the experimental particle yields. We consider how the differences in strangeness yield, at RHIC and LHC, influence physical observables, and compare how, *e.g.*,  $K^+/\pi^+$  changes between these two environments in subsection IV A. We apply the insights gained in study of thermal strangeness product in to evaluate thermal charm production at the RHIC and the LHC environments in subsection IV B.

## II. REMARKS ABOUT STRANGENESS PRODUCTION AND DENSITY

### A. Parton equilibration and strangeness production

The total final state hadron multiplicity is a measure of the entropy  $S$  produced prior to thermal production of strangeness  $s$  in QGP: Once a quasi-thermal exponential energy distribution of partons has been formed, the entropy production has been completed. Further evolution of the dense deconfined fireball is nearly entropy conserving, even though it is strangeness flavor producing: fusion of gluons or light quark pair annihilation into strangeness is a nearly entropy conserving process [20]. We note that, in reactions between two thermal particles into a strangeness pair, the energy content of each initial state parton is transferred to the two reaction products, so thermal partons produce thermal shape of strangeness spectrum.

The entropy produced in RHIC reactions has been evaluated in recent studies of hadron multiplicities. In Au–Au reactions at  $\sqrt{s_{NN}} = 200$  GeV one sees  $S \simeq 35,000$ . Furthermore, at central rapidity, the yield of entropy is  $dS/dy \simeq 5000$ . In the benchmark results we present for LHC, we will assume that the the central rapidity entropy yield is about 4 times greater than at RHIC.

The temporal evolution of the QGP fireball ends when the temperature has decreased to the QGP hadronization value. In the breakup of the QGP, the yields of hadrons are established, and it is rather difficult in the ensuing rather short lived evolution lasting not more than  $1.5$  fm/ $c$  to alter these yields appreciably. Thus, the hadronization volume, with the normalizing factor  $dV/dy$ , provides the normalization of hadron particle yields per unit of rapidity. The final value of  $dV(\tau_f)/dy$  is result of analysis of hadron particle yields and our model of the time dependence of  $dV(\tau)/dy$  will be constrained by the magnitude of  $dV_f/dy$  obtained in Ref. [21].

There are two separate stages of strangeness (charm) production, corresponding to the two practically distinct periods of the fireball evolution:  
a) ‘direct’ production creates a ‘background’ yield corresponding to what might be obtained in a superposition model of independent nucleon–nucleon (N–N) reactions.  
b) strangeness production in collisions between thermally

equilibrated QGP constituents.

For b) to be relevant prior formation of a thermal, deconfined quark-gluon plasma (QGP) phase is required. Without process b) the yield of strangeness should not be enhanced in A-A collisions as compared to scaled N-N reactions. We will not discuss in detail mechanisms a) of direct particle production here, our interest is restricted to (approximate) initial yields, which are the baseline for the thermal mechanisms acting in the QGP, and define the strength of any enhancement.

We note for the record, that strangeness initial production, like other relatively soft parton production processes, are believed to be due to color string breaking mechanism [22] and the Pythia 6 model of soft hadron production presumes that the relative strength of  $u : d : s$  production is  $1 : 1 : 0.3$ . The (initial) charm production is due to high energy parton collisions [23].

Our study of the thermal strange particle production processes is based on kinetic theory of particle collisions. There is considerable uncertainty about the initial momentum distributions of soft partons present in the initial state. However, two recent theoretical studies argue that there is rapid thermalization. The nonlinear gluon production processes leads to the gluon momentum distribution equilibration [13]. Axial asymmetry of the initial state causes collective instabilities which further accelerate thermalization of partons [24].

In this context, it is important to advance one result of our study, namely that there is little sensitivity to the initial thermal condition: a wide range of ‘reasonable’ initial temperatures leading to very similar strangeness production results, as long as the entropy content is preserved. In order to understand this, consider a decrease in initial temperature. This requires at fixed entropy an increase in initial volume, and this then is associated with increased lifespan of the fireball in the high temperature strangeness producing domain. These two effects combine to compensate the reduced strangeness production rate per unit of time and volume that is associated with reduced ambient temperature.

We believe that this mechanism also implies that the precise form of the momentum spectrum of the initial state partons is of minor practical relevance for the purpose of evaluation of strangeness production and we do not study this. Therefore, without loss of generality, we can assume that the parton distributions we use in the kinetic strangeness formation process have thermal shape, and the ambient temperature is determined considering (lattice fitted) equations of state relation of initial temperature and entropy density [25], for a given geometric initial volume.

We already remarked above that the production of strangeness in a cascade of N-N reactions (without deconfinement) is not able to add significantly to the initial strangeness yield considering the short lifespan of the fireball. Thus, this alternative will not be further considered in this work. Similarly, any additional strangeness produced in the rapid hadronization of QGP into hadrons

must be negligible compared to the thermal production process which occurs at higher particle density (temperature), and during a considerably longer lifespan.

## B. Approach to chemical equilibrium

It has been shown, considering the entropy maximization principle, that the approach of particle densities to chemical equilibrium density  $\rho_i^\infty$  can be characterized by the statistical parameter  $\gamma_i$  [26], which varies with the local proper time  $\tau$  during the collision. For example, for gluons,

$$\rho_g(\tau) \equiv \int d^3p \frac{\gamma_g(\tau) e^{-E/T}}{1 - \gamma_g(\tau) e^{-E/T}}, \quad E = \sqrt{m^2 + p^2}. \quad (1)$$

Generally, the lagrangian mass of gluons is zero. However, one may be tempted to think that thermal mass  $m(T)$  could change decisively results, suppressing the collisional strangeness production. However, one finds that instead the process of gluon decay becomes relevant and if at all, there is a net rate increase of strangeness production [27]. One could argue that the scheme to study strangeness equilibration using thermal mass amounts to a different resummation of reaction processes. In this work, we will consider the evolution of  $\gamma_s^{\text{QGP}}(\tau)$  based on lagrangian masses, allowing for  $\gamma_g^{\text{QGP}}(\tau)$  and  $\gamma_q^{\text{QGP}}(\tau)$ .

For strange quarks, we will keep only the Boltzmann term (ignoring the denominator in Eq. (1) above) and thus:

$$\rho_s(\tau) \equiv \gamma_s^{\text{QGP}}(\tau) \rho_s^\infty = \gamma_s^{\text{QGP}} \frac{g_s}{2\pi^2} z^2 K_2(z), \quad z = \frac{m_s}{T}. \quad (2)$$

Here,  $g_s$  is the strange quark degeneracy, and  $K_2$  is a Bessel function. Since we will employ strangeness occupancy in hadron phase,  $\gamma_s^h$ , we have included here the subscript QGP. We will henceforth drop this subscript, and occupancy parameters without superscript will, in general, refer to the QGP phase, while the hadronic gas phase variable, when these are expected to differ from QGP, will have a superscript ‘h’.

Our target variable is the final QGP state specific yield of strangeness per entropy,  $s/S$ , and the related phase space occupancy  $\gamma_s$ . Both these variables have an important physical relevance:  $s/S$  determines the final yield of strange hadrons compared to all hadrons, and thus its value implies some particular yield of reference yields, such as, *e.g.*,  $K^+/\pi^+$ .  $\gamma_s$  characterizes the approach to chemical equilibrium, it measures strangeness yield in terms of the chemical equilibrium yield. The strangeness phase space of QGP and HG phases are different. Strangeness in QGP is much denser than in the HG phase, considering the range of strange quark masses,  $0.080 < m_s(2 \text{ GeV}) < 0.125 \text{ GeV}$ . Therefore, (near) chemical strangeness equilibrium in the QGP phase  $\gamma_s \simeq 1$ , implies a significantly oversaturated hadron phase space abundance  $\gamma_s^h > 1$  after hadronization.  $\gamma_s^h$  is directly controlling the relative yields of hadrons with different  $s + \bar{s}$  valance quark content and is thus observable.

### C. Role of initial conditions

We do not understand well the conditions in the QGP phase at the time as early as  $\tau_0 = 0.25$  fm for RHIC and  $\tau_0 = 0.1$  fm for LHC when we presume that the thermal momentum distribution is practically established. Thus, we must make a number of assumptions and check if these impact our results. The relevant parameters that could govern the strangeness production are:

$\gamma_g(\tau)$ , and in particular the initial value at  $\tau_0$ ;  
 $\tau_0$ , the time at which we assume thermal momentum of partons is reached.  
 $s/S|_{\tau_0}$  is the initial strangeness yield originating in direct parton collisions.

$R_\perp$  is the transverse radius dimension at initial time, related to the collision geometry

$v_\perp(\tau)$  is the transverse expansion velocity, and in particular its maximum value at hadronization.

$\tau_g$  and  $\tau_q$ , the relaxation time constant of gluon and quark fugacities, considering that quarks are less relevant compared to gluons with regard to strangeness production, we will assume  $\tau_q=1.5 \tau_g$  throughout this work.

We explore here a characteristic gluon thermalization time  $0.1 < \tau_0 < 1.5$  fm/c with the longest value applicable to most peripheral RHIC Au–Au reactions at  $\sqrt{s_{\text{NN}}} = 200$  GeV and the shortest period assumed for the future Large Hadron Collider (LHC) central collisions. What exactly the dynamics of thermalization is and how long it takes will as we shall see rather unimportant for the final insights we obtain.

All initial state parameters are constrained in their value, either by collision geometry, by final state particle yields observed at RHIC, or/and by particle correlations. For example, the final yield of strangeness  $ds/dy$  and of entropy  $dS/dy$ , and thus  $s/S$  are known from an analysis of particle production: as function of centrality at RHIC [21] and as function of reaction energy from top AGS, SPS to top RHIC energy [28].

We will use these results in two ways. We compute, following the temporal evolution, the final state  $s/S$  ratio which we expect to converge at RHIC to  $s/S \simeq 0.027$ . We need to specify the initial value at time  $\tau_0$  for this variable, and this value is chosen to be compatible with the peripheral reactions. The entropy yield  $dS/dy$ , which we assume is conserved during the evolution of QGP, determines, for a known initial volume  $dV(\tau = \tau_0)/dy$ , the entropy density  $\sigma = (dS/dy)/(dV/dy)$ . We then can obtain from standard properties of QGP fitted to the lattice results the initial temperature  $T_0/T_c \simeq 3–4$ . This temperature decreases as volume expands with  $\tau$  given that the entropy is preserved.

We will show that the two physical observables,  $s/S$  and  $\gamma_s$ , we address are largely independent of the model dependent details of the initial conditions. Said differently, our important finding is that the two global strangeness observables  $s/S$  and  $\gamma_s$  appear to penetrate back only to about 2 fm/c after the reaction has begun, and do not probe earlier conditions in the QGP phase.

The physical reason for this is, of course, that once chemical equilibrium is approached, one loses much of the event memory with regard to intensive physical observables. We will further see that, in cases we studied, that did not quite reach chemical equilibrium in the QGP phase, this is also true, *i.e.*, there is little sensitivity to what exactly happened to light quarks and gluons in the first 2 fm/s.

The reason for this is that there is a strong correlation between volume, temperature and degree of QGP (gluon and light quark) chemical equilibration as we already discussed above. Repeating the argument differently, when there are fewer gluons at fixed entropy in given volume, temperature has to be larger. Thus, any decrease in the production of strangeness in gluon fusion due to absence of gluons is compensated by the greater specific rate per colliding pair due to greater ambient temperature. Hence, also when we do not quite reach chemical equilibrium in QGP, be it due to large impact parameter or low reaction energy (chemical nonequilibrium at lower energies is not explored in this paper), there is little if any dependence of thermal yield on initial conditions, and the results we arrive at regarding near chemical equilibration are extraordinarily robust.

However, the thermal strangeness production does depend on the degree of initial state strangeness equilibration, simply because if the initial yields were chemically equilibrated to start with, there would be as much production as annihilation of strangeness and any temporal evolution is driven by the time dependence of the evolution dynamics. We will take as a measure of the pre-QGP thermal phase strangeness production the specific per hadron multiplicity yield of strangeness observed in most peripheral RHIC reactions. This is typically  $s/S \simeq 0.016$  at  $\tau = \tau_0$ . This choice allows to reproduce the observed value  $s/S = 0.019$  attained in most peripheral nuclear reactions at RHIC [21], with participant number about  $\langle A \rangle = 6.3$ . Clearly, with  $s/S \rightarrow 0.27$  in most central collisions, the implication of this choice is that the thermal process enhances total specific yield by factor  $1.9 \pm 0.3$ . As centrality and/or reaction energy decreases, there is a gradual decrease of this enhancement, and as the energy is increased (LHC) this enhancement rises somewhat.

### D. Thermal strangeness production

We follow the established methods of evaluating thermal strangeness production [29], expanding our earlier more schematic model [30]. However, considerable simplification arises since we focus attention on the specific yield of strangeness per entropy.

In the local (comoving) frame of reference, the rate of change of strangeness is due to production and annihilation reactions only:

$$\frac{1}{V} \frac{ds}{d\tau} = \frac{1}{V} \frac{d\bar{s}}{d\tau} = \frac{1}{2} \rho_g^2(t) \langle \sigma v \rangle_T^{gg \rightarrow s\bar{s}} + \rho_q(t) \rho_{\bar{q}}(t) \langle \sigma \rangle_T^{q\bar{q} \rightarrow s\bar{s}}$$

$$-\rho_s(t) \rho_{\bar{s}}(t) \langle \sigma v \rangle_T^{s\bar{s} \rightarrow gg, q\bar{q}}. \quad (3)$$

The thermally average cross sections are:

$$\langle \sigma v_{\text{rel}} \rangle_T \equiv \frac{\int d^3 p_1 \int d^3 p_2 \sigma_{12} v_{12} f(\vec{p}_1, T) f(\vec{p}_2, T)}{\int d^3 p_1 \int d^3 p_2 f(\vec{p}_1, T) f(\vec{p}_2, T)}. \quad (4)$$

$f(\vec{p}_i, T)$  are the relativistic Boltzmann/Jüttner distributions of two colliding particles  $i = 1, 2$  of momentum  $p_i$ , characterized by local statistical parameters.

A convenient way to address the dilution phenomena acting on the density of strangeness  $\rho_s \equiv s/V$  due to rapid expansion of the QGP phase, Eq. (3), is to consider the proper time evolution of the specific strangeness per entropy yield:

$$\frac{d}{d\tau} \frac{s}{S} = \frac{V}{S} \frac{1}{V} \frac{ds}{d\tau}. \quad (5)$$

The entropy  $S$  in a volume element is unchanged, as volume grows and temperature drops:

$$S = V \frac{4\pi^2}{90} g(T) T^3 = \text{Const.}, \quad (6)$$

where we consider the quark and gluon degrees of freedom along with their QCD corrections:

$$g = 2_s 8_c \left( 1 - \frac{15\alpha_s(T)}{4\pi} + \dots \right) + \frac{7}{4} 2_s 3_c n_f \left( 1 - \frac{50\alpha_s(T)}{21\pi} + \dots \right). \quad (7)$$

We use as the number of quark flavors  $n_f \simeq 2 + \gamma_s 0.5z^2 K_2(z)$ , where  $z = m_s/T$ . The terms proportional to chemical potentials are not shown in the expression for entropy, since  $\mu/\pi T \ll 1$  at RHIC and LHC.

In order to use the detailed balance which relates production and annihilation reactions, it is convenient to introduce the invariant rate per unit time and volume,  $A^{12 \rightarrow 34}$ , by incorporating the equilibrium densities into the thermally averaged cross sections:

$$A^{12 \rightarrow 34} \equiv \frac{1}{1 + \delta_{1,2}} \gamma_1 \gamma_2 \rho_1^\infty \rho_2^\infty \langle \sigma_s v_{12} \rangle_T^{12 \rightarrow 34}. \quad (8)$$

Here,  $\delta_{1,2} = 1$  for the reacting particles being identical bosons, and otherwise,  $\delta_{1,2} = 0$ . Note also that the evolution for  $s$  and  $\bar{s}$  in proper time of the comoving volume element is identical as both change in pairs.

We find that the temporal evolution of  $s/S$  in an expanding plasma is governed by:

$$\frac{d}{d\tau} \frac{s}{S} = \frac{A^{gg \rightarrow s\bar{s}}}{(S/V)} [\gamma_g^2(\tau) - \gamma_s^2(\tau)] + \frac{A^{q\bar{q} \rightarrow s\bar{s}}}{(S/V)} [\gamma_q^2(\tau) - \gamma_s^2(\tau)]. \quad (9)$$

When all  $\gamma_i \rightarrow 1$ , the Boltzmann collision term vanishes, we have reached equilibrium. The value arrived at for the

observable  $s/S$  depends on the history of how the system evolves and, eventually, reaches equilibrium.

In order to be able to solve Eq. (9), we need a relation between  $s/S$  and  $\gamma_s$ . This is obtained combining strangeness density Eq. (2) and entropy Eq. (6):

$$\frac{s}{S} = \gamma_s \frac{g_s}{g} \frac{90}{8\pi^4} z^2 K_2(z), \quad z = m_s/T. \quad (10)$$

In the initial period, gluons and quarks have not reached chemical equilibrium, thus the actual numerical integrals of Bose and Fermi distributions of the type Eq. (1), dependent on the values  $\gamma_{q,g}$  are employed instead which modify the result seen in Eq. (10).

The degeneracies we have considered in Eq. (6) for the entropy did include the effect of interactions, and thus, we have to allow for the interaction effect in the strange quark degeneracy as well:

$$g_s = 2_s 3_c \left( 1 - \frac{k\alpha_s(T)}{\pi} + \dots \right). \quad (11)$$

The value of  $k = 2$  applies to massless strange quarks. At  $T = 0$  (or said differently, for  $m \gg T$ ) the early study of quark matter self-energy suggests that  $k \rightarrow 0$  [31]. We will present, in figure 5 below, results varying the value of  $k$ , and the reference value we use in our other studies is  $k = 1$ .

We evaluate  $A^{gg \rightarrow s\bar{s}}$  and  $A^{q\bar{q} \rightarrow s\bar{s}}$  employing thermal strength of the QCD coupling and thermal quark mass, see [3]. To determine the strength of the QCD coupling constant as function of the energy scale, we take as reference value  $\alpha_s(\mu = m_{Z^0} = 0.118)$ , and evolve the value to applicable energy domain  $\mu$ . We express  $\alpha_s$  as function of temperature by the conditions  $\alpha_s(T) = \alpha_s(\mu = 2\pi T)$ . This results in the expression (see section 14 in [29]):

$$\alpha_s(T) \simeq \frac{\alpha_s(T_c)}{1 + C \ln(T/T_c)}, \quad T < 5T_c, \quad (12)$$

with  $C = 0.760 \pm 0.002$ ,  $\alpha_s(T_c) = 0.50 \pm 0.04$  at  $T_c = 0.16$  GeV. We allow the mass of strange quarks to run and use  $m_s(T) \equiv m_s(\mu = 2\pi T)$ . Since the running of mass involves a multiplicative factor, the uncertainty in the mass value remains factorial. We employ here the central value from the PDG evaluation,  $m_s(\mu = 2\text{ GeV}) = 0.10$  GeV which remains uncertain at the level of 25% at least. We will consider the influence of this uncertainty in more detail. see figure 6 below.

## E. Expansion and cooling of QGP

We separate, in our work, the issue of strangeness production from the even more complex and less understood questions about the time evolution of the QGP. We assume that there is some active volume at average temperature  $T$ , in which the strangeness is ‘cooked’. We derive the time dependence of local temperature from the hypothesis of a conserved entropy content and a reasonable

model describing the volume evolution in time. This is arrived at using a hydrodynamical inspired model.

The volume at hadronization is an implicit observable. All particle yields at hadronization are normalized with a volume factor. Thus, our expansion model must be realistic enough so that the hadronization conditions are in agreement with data and, that the impact parameter dependence is reproduced. In the geometry inspired model we consider, in the central rapidity domain:

$$\frac{dV}{dy} = A_{\perp}(\tau) \frac{dz}{dy} \Big|_{\tau=\text{Const.}}. \quad (13)$$

$dV/dy$  is the normalization factor for the particle yields we are measuring in an interval around central rapidity. The transverse expansion is described by the transverse size  $A_{\perp}(\tau)$ . We further need to associate with the domain of rapidity  $dy$  a geometric region at the source  $dz$ , from which particles emerge.

To accomplish this, we recall the space-time rapidity of the scaling Bjørken hydrodynamical solution:

$$y = \frac{1}{2} \ln \frac{t+z}{t-z}. \quad (14)$$

We see that  $y=0$  corresponds to  $z=0$ . In particular, if the transverse extend of the fireball is large, the Bjørken space-time rapidity relation prevails.

We need this relation not at a fixed laboratory time  $t$  but at some fixed proper time  $\tau$ :

$$\tau = \sqrt{t^2 - z^2}. \quad (15)$$

We eliminate in Eq. (14)  $t$  using Eq. (15):

$$z = \tau \sinh y, \quad \frac{dz}{dy} = \tau \cosh y. \quad (16)$$

$A_{\perp}$  is the transverse to scattering axes size of the evolving QGP. For nearly homogeneous expanding bulk matter one can assume:

$$A_{\perp} = \pi R_{\perp}^2(\tau). \quad (17)$$

However, if the matter is predominantly concentrated near a narrow domain of width  $d$ , we consider:

$$\begin{aligned} A_{\perp} &= \pi [R_{\perp}^2(\tau) - (R_{\perp}^2(\tau) - d)^2] \\ &= 2\pi d \left[ R_{\perp}(\tau) - \frac{d}{2} \right]. \end{aligned} \quad (18)$$

Thus, at central rapidity, we consider quantitatively the two evolution scenarios, denoted hereforth as models V1 and V2. V1 will be the most simple bulk homogeneous expansion while model V2 simulates a transverse donut, it corresponds to expansion with a cold hole of matter in fireball (axial) center:

$$\text{V1 : } \frac{dV}{dy} = \pi R_{\perp}^2(\tau) \tau, \quad (19)$$

$$\text{V2 : } \frac{dV}{dy} = 2\pi d \left[ R_{\perp}(\tau) - \frac{d}{2} \right] \tau, \quad (20)$$

with

$$R_{\perp}(\tau) = R_0 + \int v(\tau) d\tau. \quad (21)$$

Any model of transverse matter expansion dynamics  $v(\tau)$  is constrained by the transverse mass shape of produced particle spectra, too large transverse velocities would produce too hard spectra. Accordingly, a hydro-inspired shape is assumed:

$$v(\tau) = v_{\max} \frac{2}{\pi} \arctan[4(\tau - \tau_0)/\tau_v]. \quad (22)$$

Values of  $v_{\max}$  we consider are in the range of 0.5–0.8c, the relaxation time  $\tau_c \simeq 0.5$  fm, and the onset of transverse expansion  $\tau_0$  was tried in range 0.1–1 fm. None of these parameters matters for what follows as long as one does not employ aberrant values.

The initial size  $R_{\perp}$  is assumed, in what follows, to be  $R_{\perp} = 5$  fm for 5% most central collisions. When we study centrality dependence, we will show results for a series of centralities decreasing the transverse dimensions  $R_{\perp}$  and  $d$  by factor  $f_R = 1.5$  in each step. We further scale entropy value with  $f_S = f_R^{2.2}$ . This assures that the dependence of entropy on the participant number  $dS(A)/dy$  in the final state follows the relationship,

$$\frac{dS}{dy} \simeq 8(A^{1.1} - 1), \quad (23)$$

obtained from the impact parameter dependent fit to the RHIC impact parameter results [21].

An overview of the resulting volume dynamic behavior is given in figure 1, the top panel applies to RHIC with  $\sqrt{s_{\text{NN}}} = 200$  GeV, the bottom panel presents a parallel study for LHC with the *assumed* four times greater entropy content. The solid lines are for transverse homogeneous volume (V1 model) expansion, and dashed lines correspond to a transverse region of thickness  $d = 3.5$  fm (V2 model).

Three different centralities were considered with  $R_{\perp} = 3, 5$  and 7 fm. For the second model of transverse expansion, the transverse size  $d$  is scaled with  $R_{\perp}/5$  fm. Thus,  $d = 2.1$  fm for  $R_{\perp} = 3$  fm and  $d = 4.9$  fm for  $R_{\perp} = 7$  fm. Similarly, entropy content, assumed to be  $dS/dy = 5000$  at RHIC and  $dS/dy = 20,000$  at LHC for  $R_{\perp} = 5$  fm, is scaled to values  $dS(R_{\perp} = 3 \text{ fm})/dy = 1300$  and  $dS(R_{\perp} = 7 \text{ fm})/dy = 10,500$ , and correspondingly, 4 times greater values for LHC.

The temporal expansion of the volume is followed till  $T = 140$  MeV is reached. In general, the maximum volume at LHC is thus 4 times greater compared to RHIC. The expansion time is correspondingly longer, with RHIC taking 6.5 fm to freeze-out for  $R_{\perp} = 5$  fm, the LHC lifespan is 10 fm. The QGP lifespan increase by as much as 60% at LHC, when comparing to RHIC, if the assumed initial entropy production is indeed increased by factor 4. From the perspective of strangeness production, this is one of the more interesting changes comparing RHIC to LHC.

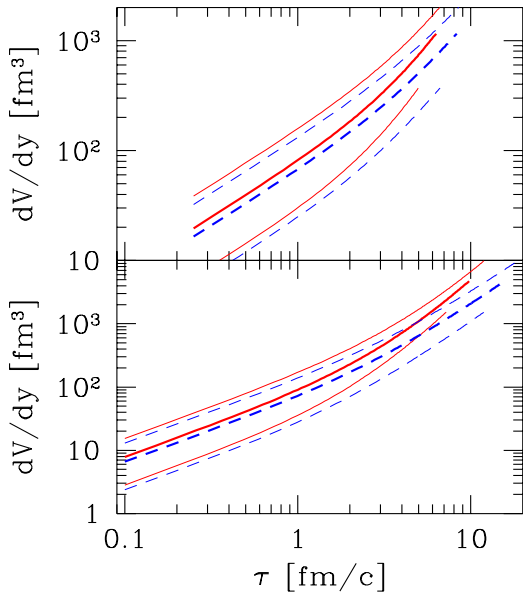


FIG. 1: (color online) QGP Volume related to central rapidity,  $dV/dy$  as function of proper time  $\tau$ . Top panel is for RHIC with reference entropy content  $dS/dy = 5,000$  (central lines), while bottom panel is for LHC with 4 times greater entropy content  $dS/dy = 20,000$  (central lines). Three centralities are considered, with the middle thicker lines corresponding to  $R_\perp = 5$  fm and the upper/lower lines corresponding to  $R_\perp = 7$ , and, respectively,  $R_\perp = 5$  fm/c. Solid lines are for V1 model with transverse homogeneity, dashed lines for V2 model of a transverse shell with widths (top to bottom)  $d = 2.1, 3.5$  and  $4.9$  fm. The volume expansion is shown in the figure up to  $T = 140$  MeV. See text for more details.

Given the volume as function of  $\tau$ , and the associated conserved entropy content, we can evaluate the prevailing temperature  $T$  for any given quark and gluon chemical equilibration condition  $\gamma_{q,s,g}$ . The solid lines in top panels of the following figures 2 to 6 show this result, in the figures 2 and 3, on left for the V1 model and on right for the V2 (donut) model. The assumed  $\gamma_g$  is presented as dashed line. In some of the top panels, we also show by the dotted line the time dependence of the applied transverse velocity,  $v_\perp$ , see Eq. (22).

### III. RESULTS ON STRANGENESS PRODUCTION

#### A. The benchmark results for RHIC

We show, in figure 2, a survey of the results which the approach we discussed produce. In this and several following figures 3, 4, 5 and 6, in which will explore the dependence on the initial assumptions made, we in general show three panels above each other, and side to side the two volume models, see Eqs. (19 and 20), on left V1 and on right (donut model) V2 (figures 3 and 4). In figures 5 and 6, we show side to side RHIC (on left) and

LHC (on right). As noted already, in the top panel, we show by solid line(s) the model time temperature profiles. The experimental observables are shown also as solid line(s) in the middle panel ( $\gamma_s$ ) and in the bottom panel ( $s/S$ ). The other lines illustrate as appropriate the key inputs used to obtain these results. When several lines of the same type are present, we are presenting the impact parameter dependence, scaling the size and entropy content as discussed above. In general, the temperature is followed down to a freeze-out at  $T_f = 0.14$  GeV.

In figure 2, we show the most likely result of our study for RHIC centrality dependence at 100+100 GeV. The solid lines in the top panels show 6 different centralities, with the lowest temperatures seen for the least central collisions, all temperatures continue to  $T = 0.14$  GeV. The slight increase in the initial temperature with increasing centrality is result of the scaling of initial entropy which accommodates the observed change in  $dS/dy|_f$  beyond participant scaling, see Eq. (23). All lines shown begin at  $\tau_0 = 1/4$  fm, where the initial temperatures range  $T_0 \in (0.55, 0.6)$  GeV. For the V1 model, the lifespan of proper life spans the interval  $\tau_f = 2.2$  fm (most peripheral) to  $\tau_f = 6.5$  fm (most central). In the donut expansion model V2, the range is from  $\tau_f = 3$  to 8 fm.

In the top panel, we also show the growth with  $\tau$  of the transverse expansion velocity (dotted line), and the pair threshold using running strange quark mass,  $2m_s^r$  (dashed lines). We note that the temperature drops below the pair threshold for the most peripheral reactions considered already at  $\tau = 1$  fm/c, and this occurs for the most central reactions at  $\tau = 2$  fm/c (model V1) and respectively, 1.5 and 2.8 fm/c for model V2. Thus, high strength thermal strangeness production life span varies by as much as factor 3, depending on centrality, and the expansion model.

In the middle panel, we show dashed the rise of the gluon occupancy  $\gamma_g$  which we employed. The quark occupancy  $\gamma_q$  is following the same functional temporal evolution starting with 2/3 smaller initial value and evolving with a time constant 1.5 times slower. Because gluons dominate strangeness production in QGP, we do not show this quark property in detail. The dotted lines show how the volume evolves toward its maximum value at freeze-out. Each line is normalized to unity at freeze-out. The actual value of the volume can be read of the figure 1, given the value of  $\tau$ .

In summary of the key results: we see a gradual increase with centrality of strangeness, for V1:  $s/S \rightarrow 0.028$  and  $\gamma_s \rightarrow 0.8$ , for V2:  $s/S \rightarrow 0.030$  and  $\gamma_s \rightarrow 0.85$ . There near strangeness saturation at RHIC. More detailed discussion will be presented further below.

#### B. Strangeness production predictions for LHC

We perform a similar evaluation of strangeness production for LHC. To account for the greater reaction

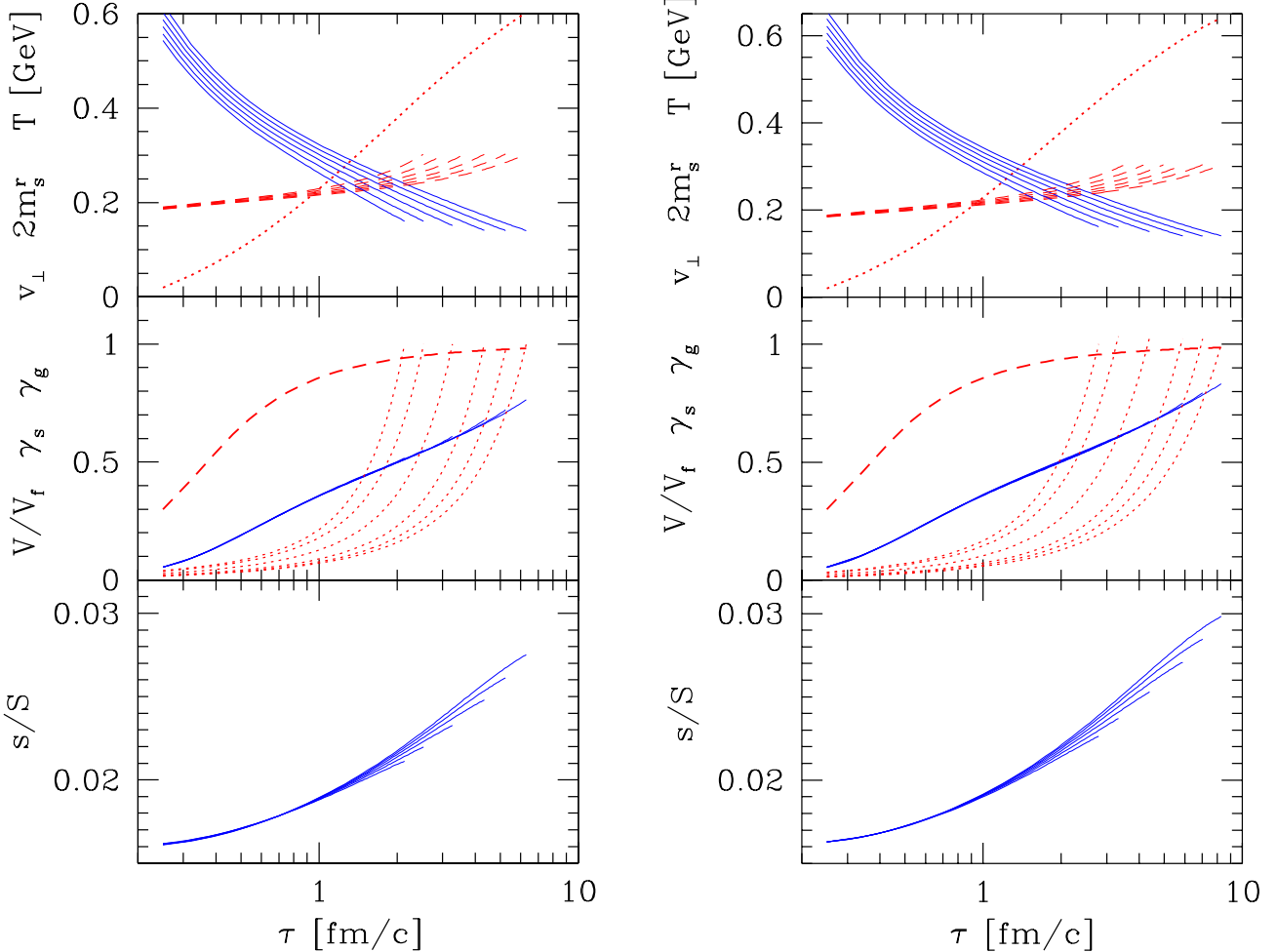


FIG. 2: (color online) Comparison of the two transverse expansion models, see Eqs. (19,20): left bulk expansion (model V1), right donut expansion (model V2). Different lines correspond to different centralities. Top panel: solid lines: temperature  $T$ ; dashed lines: running mass  $m_s^r(T)$ ; dotted line: the assumed profile of transverse expansion velocity  $v_\perp(\tau)$ . Middle panel: Solid line(s)  $\gamma_s$ , which nearly coincide for different centralities; dashed, the assumed  $\gamma_g(\tau)$ , dotted the profile of the assumed volume,  $[dV(\tau)/dy]/[dV(\tau_f)/dy]$  normalized by the freeze-out value.  $R_\perp(\tau_0)$  stepped down for each line by factor 1.5. The end points, at maximum  $\tau$ , allow to find corresponding centrality curves. Bottom panel: resulting  $s/S$  for different centralities. The initial temperatures change slightly to accommodate an observed change in  $dS/dy|_f$  beyond participant scaling, see Eq. (23).

energy, as already noted we increase the entropy content by factor 4, which implies an assumed increase in rapidity density of hadrons by a similar factor. We assume that in elementary parton interactions the relative strength of strangeness and non-strange hadron production is unchanged and thus, we keep the initial relative yield  $s/S = 0.016$  constant. Given the entropy yield increase, we implicitly assumed an increase in absolute strangeness yield by factor 4 at LHC compared to RHIC.

We further assume that thermalization time has dropped from  $\tau_0 = 1/4$  fm at RHIC to  $\tau_0 = 1/10$  fm at LHC. However, inspecting the slowly changing initial state evolution, in figure 3, there would be little change in our results, were  $\tau_0$  remain unchanged between RHIC and LHC. At this early, time  $\tau_0 = 1/10$ , the value of  $\gamma_s(\tau_0)$  at LHC is similar to the situation at RHIC, compare the beginning of the solid line in middle panel of figures 2 and 3. This is so, since the magnitude of the

phase space scales with  $T^3$  and the initial temperature  $T(\tau_0)$  is considerably greater at LHC: in the top panel, in figure 3, we see that it reaches up to  $T = 1.25$  GeV. For this reason, we have to show in the top panel (dashed lines)  $5m_s^r$  rather than  $2m_s^r$ , in order to fit it visibly into the top panel of the figure, and this is the only difference in the display of LHC results, in figure 3, as compared to the RHIC results, figure 2.

In order to accommodate the greater transverse expansion pressure, we increased the maximum transverse flow velocity which can now attain  $v_\perp = 0.80c$  (dotted line, top panel figure 3). Despite this, the evolution time at LHC is significantly longer, with the most central collisions taking up to 30% longer to reach the freeze-out temperature,  $T_f = 0.14$  GeV. The reader who prefers earlier freeze-out, at, *e.g.*,  $T_f = 0.17$  GeV can evaluate the changes required by consulting the temperature profiles shown in the top panel.

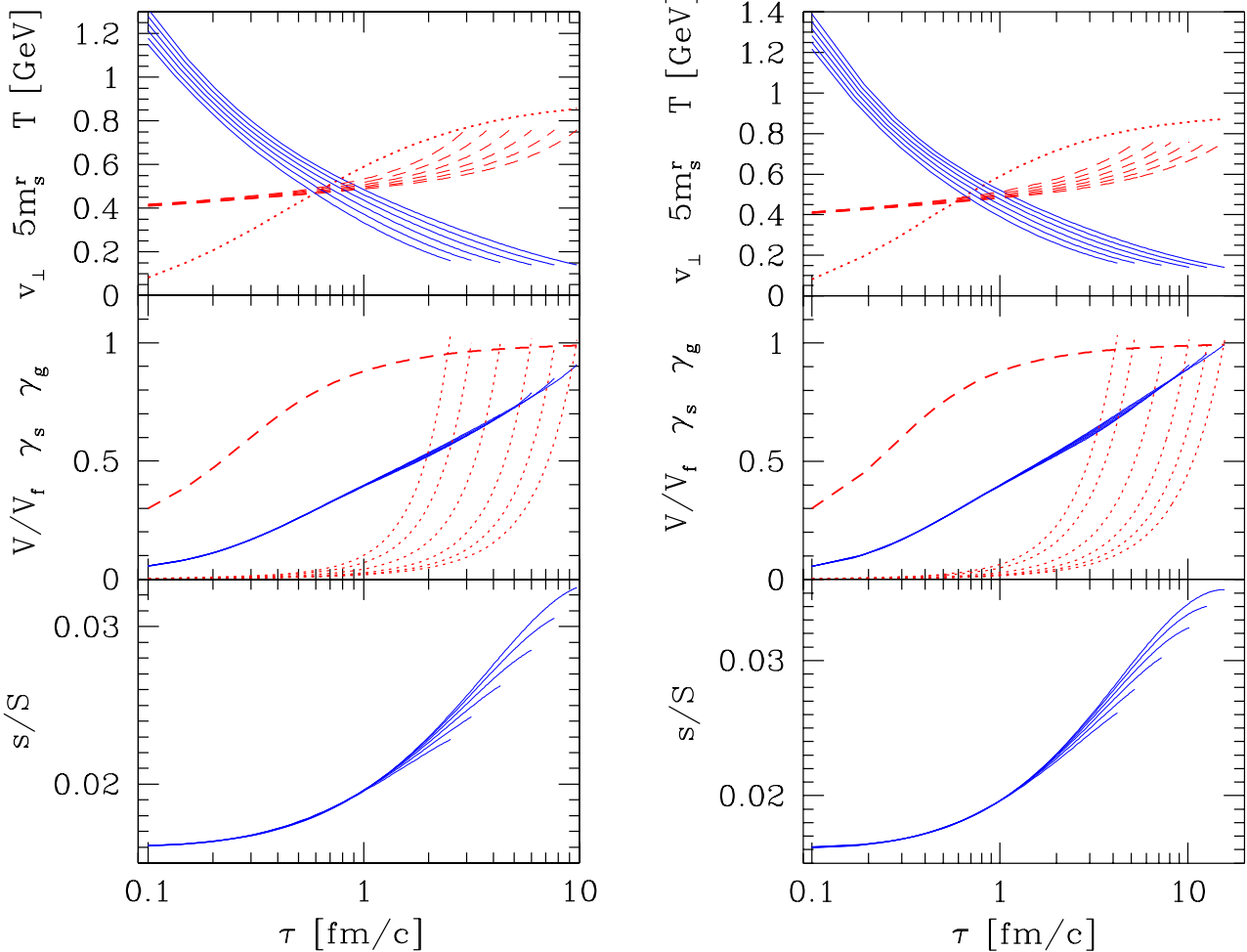


FIG. 3: (color online) Same as in figure 2 for the case of LHC, with same initial  $s/S = 0.016$ , but entropy content (hadron multiplicity) being 4 times greater compared to RHIC. See text for more details.

The different centralities, at LHC, are considered with the same scaling of the transverse size and entropy content as we did for the case of RHIC. Comparing the left to right set of results (*i.e.*, volume V1 to donut V2 expansion models) for LHC, we see a more developed chemical equilibrium of strangeness with clear evidence of (over)saturation of yields for a few centralities, see the bottom panel on right in figure 3. There is greater final specific strangeness content at LHC than at RHIC, with visibly greater thermal production leading to strangeness (over)saturation. At RHIC, the thermal production raises the value of  $s/S$  from 0.016 to 0.028 for most central collisions (V1 model of bulk volume expansion), while at the LHC the thermal production raises  $s/S$  from 0.016 to 0.032. We will discuss below what this increase means for the  $K/\pi$  ratio. The same relative increase in  $s/S$  is seen in the model V2 of the expansion comparing RHIC and LHC. However, if the homogeneous bulk expansion applies at RHIC, but a donut type expansion arises at LHC, the increases in strangeness yield and lifespan would be more spectacular. Depending on its expansion dynamics, LHC clearly harbors the potential to surprise us.

### C. Study of the dependence on initial thermalization condition

An important question, which we address next, is how variation of the initial conditions impacts the results we presented above. We have studied this question in depth in many different model approaches. The answer ‘practically no dependence’ is best illustrated in the figure 4, where we show the more conservative volume expansion model V1 results on left for RHIC, and on right for LHC. We explore a wide range of initial gluon (and quark) occupancy  $\gamma_g$ , which for consistency with other figures is shown in the middle panel by dashed lines, the initial values we consider for glue occupancy vary as  $0.1 < \gamma_g(\tau_0) < 2.1$  in step of 0.5. The second of these lines, from the bottom, is the reference behavior we use in figures 2 and 3.

We recall that, with  $\gamma_g(\tau_0)$ , we also vary  $\gamma_q(\tau_0)$ , which following the same functional temporal evolution starting with 2/3 smaller initial value and evolving with a time constant 1.5 times slower. Note also that the scale in top panel varies between RHIC (left) and LHC (right) cases

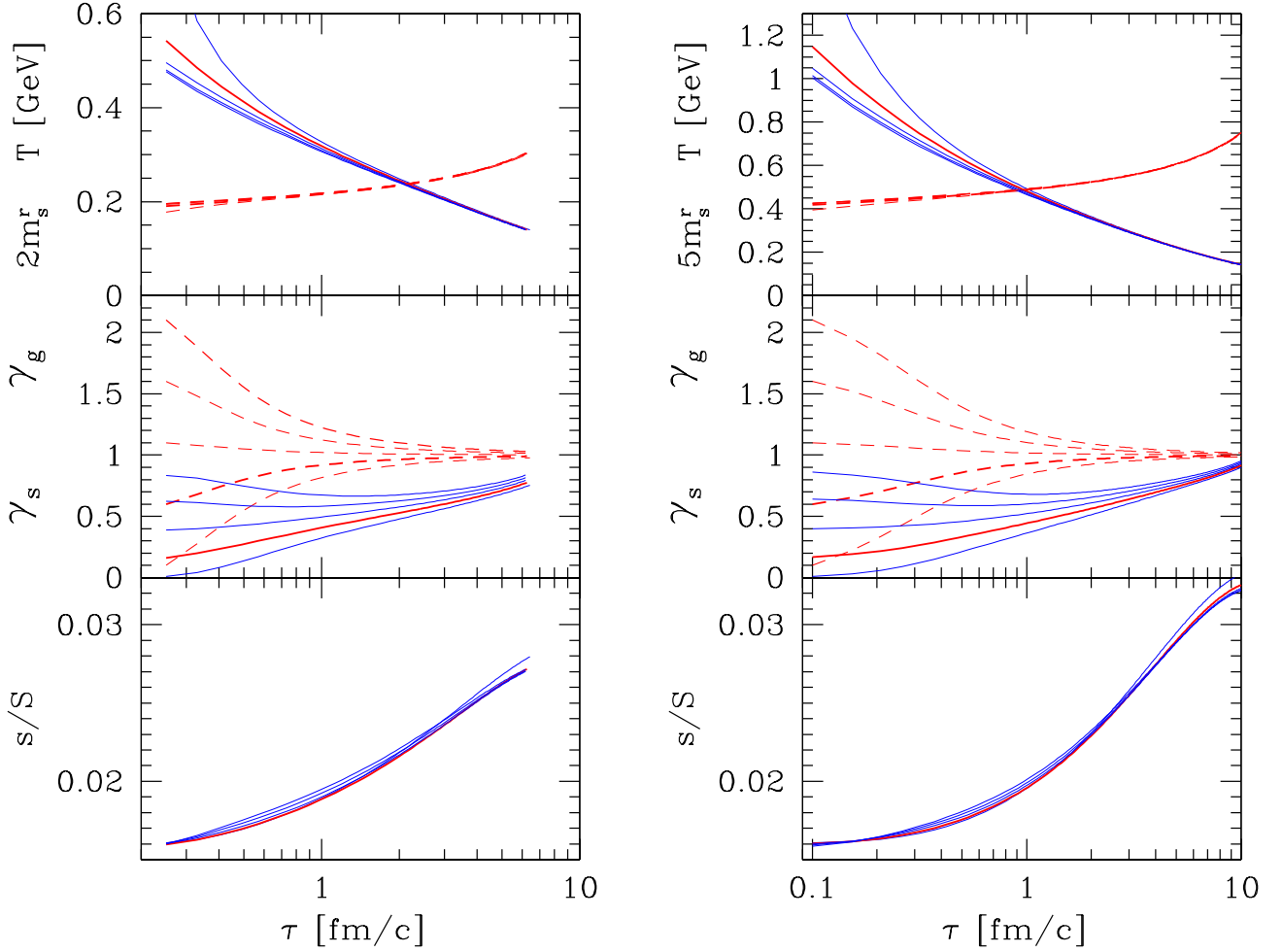


FIG. 4: (color online) Model V1 (volume expansion) at RHIC (left) and LHC (right) for 5% most central collisions.  $s/S$  (bottom panel) and  $\gamma_s$  (solid line middle panel) evolution (in)dependence of widely varying initial gluon conditions ( $T$  in top panel,  $\gamma_g$  dashed middle panel).

the dashed lines denote  $2m_s$  on left, and  $5m_s$  on right. Since the initial value of  $s/S = 0.016$  and  $dS/dy = 5,000$  (on left, RHIC) and, respectively  $dS/dy = 20,000$  (on right, LHC) is set, there is a corresponding variation in  $T_0$  (top panel, left end of solid lines) and  $\gamma_s$  (left end of solid lines in middle panel). The final results for  $\gamma_s(\tau_f)$  (right end of solid lines in middle panel) and  $s(\tau_f)/S$  (bottom panel) are impressively insensitive to this rather exorbitant diversity of initial conditions.

We conclude that strangeness cannot probe the very initial QGP conditions near  $\tau_0$  — the memory of the initial history of the reaction is lost, the system is opaque below  $\tau = 2\text{--}3 \text{ fm}/c$  to the strangeness signature. On the other hand, and most importantly for the study here undertaken, this also means that the predictions of experimental observables are characteristic of the properties of chemically equilibrated QGP. We found that only if gluons in QGP did not approach the chemical equilibrium at  $\tau_f$ , a signature of this condition would be seen in the strangeness yield as is seen considering the right hand side of Eq.(9). Correspondingly smaller value of

$s/S$  would then result.

One can safely presume, seen the amount of strangeness produced which agrees with experiment, that in most central RHIC collisions, one obtains nearly completely chemically equilibrated QGP. On the other hand, the small size and lifespan of possible QGP in peripheral collisions can imply that the system is far from chemical equilibrium, and hence the strangeness yield is suppressed in these collisions. This study shows that the (near) chemical equilibration in QGP of strangeness, and the resulting opacity of QGP, is the reason that some considerably less sophisticated models we and others have considered, as long as these yield conditions near to chemically equilibrated QGP, are equally successful in evaluating the strangeness production. However, when gluon (and light quark) chemical equilibrium is not attained even in central reactions at RHIC, as is the case, *e.g.*, in models proposed in Ref. [18, 19], there remains dependence on the history of the fireball. However, these results are offering strangeness yields below the level required by RHIC experiment.

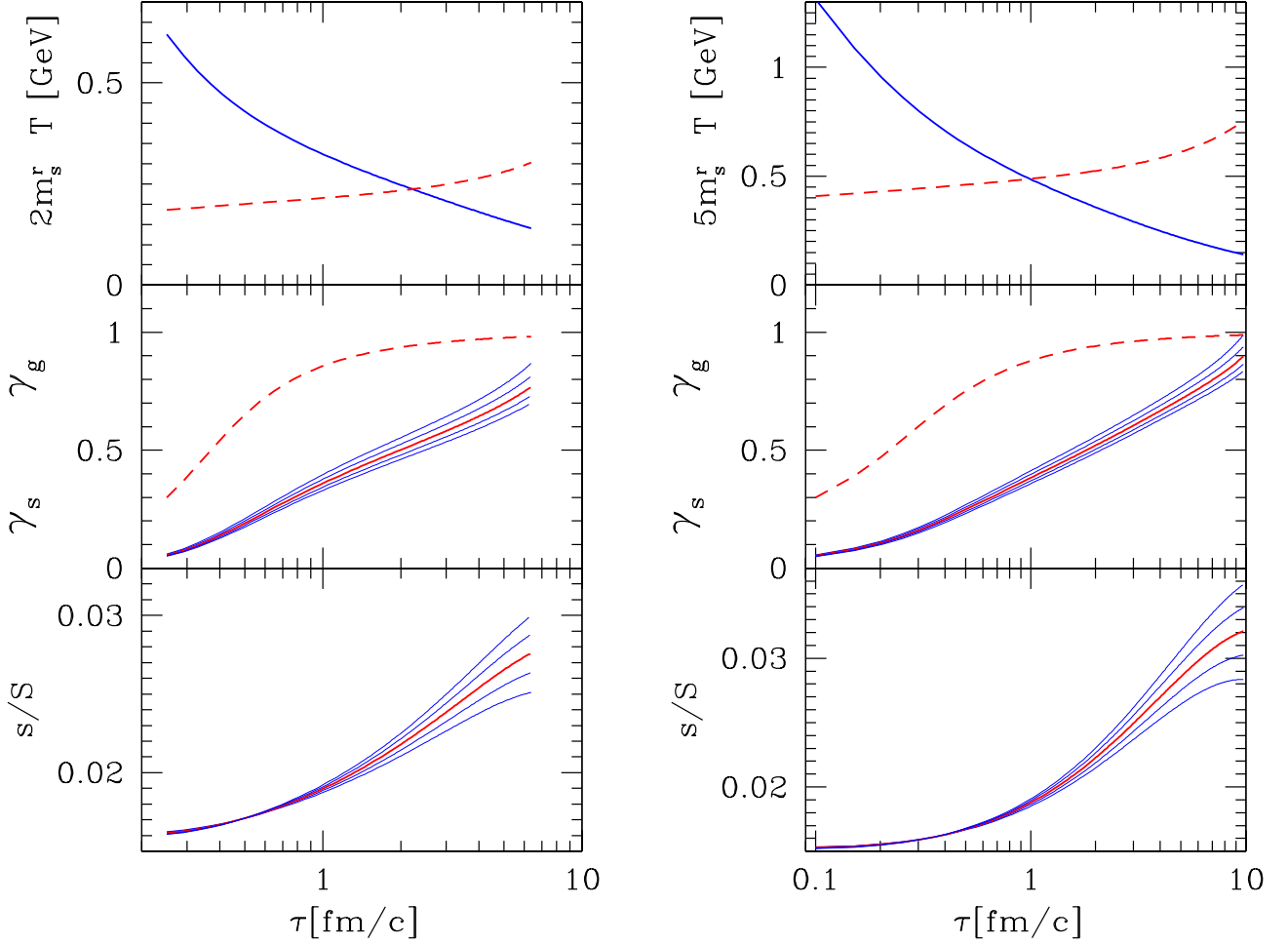


FIG. 5: (color online) Study of dependence on the perturbative QCD correction to the strange quark density, left for RHIC and right for LHC, V1 expansion model. Figure structure same as figure 4. Middle panel, solid lines: computed evolution of  $\gamma_s$  in the deconfined phase for values of  $k = 2, 1.5, 1, 0.5$  and  $0$ ; and bottom panel: corresponding evolution of  $s/S$ . The lowest  $\gamma_s$  line corresponds to  $k = 0$  and the largest to  $k = 2$ , the opposite applies for  $s/S$  lines. See text for details.

#### D. Fundamental uncertainties in strangeness production

There are two QCD related uncertainties in our strangeness production study:

- 1) the effect of interaction on the number of strange quark degrees of freedom, Eq. (11), and
- 2) the value of strange quark mass.

We will show that the current uncertainties lead to observable effects, in particular regarding the final value of  $s/S$ , and to a lesser extend also regarding the chemical equilibration, the final value of  $\gamma_s$ .

To see this, we need to recall that while  $\gamma_s$  is a mathematical quantity introduced in Eq. (2) in order to relate the prevailing strangeness density to the chemically equilibrated density at temperature  $T$ , its actual value enters decisively into the kinetic equation of strangeness production. Eq. (9) shows that the smaller the value of  $\gamma_s$ , the bigger is the change in the value of  $s/S$ . In other words, when we explore the relevance of a change in the effective degeneracy, Eq. (11), at a given strangeness yield,

i.e., given  $s/S$ , we can enhance, or reduce, the expected final value of  $s/S$ , as well as  $\gamma_s$ .

Since in our approach we used Boltzmann statistics for the strangeness degree of freedom, the effect of Pauli blocking on strangeness production is not considered. The direct dependence of physical observables on  $\gamma_s$  arises from the process of strangeness reannihilation into gluons. We note that Eq. (9), describing the change in strange quark yield, can also be cast into the form:

$$\frac{d}{d\tau} \frac{s}{S} = a_g(\rho_g^2 \rho_s^{\infty 2} - \rho_s^2 \rho_g^{\infty 2}) + a_q(\rho_q^2 \rho_s^{\infty 2} - \rho_s^2 \rho_q^{\infty 2}), \quad (24)$$

where instead of  $\gamma_i$  the actual densities of particles appear. We see that for each particle both the equilibrium, and transient, density must enter in order for the system to attain chemical equilibrium as function of time. Consequently, the value of  $\gamma_s$  and hence the QCD correction in Eq. (2) matters.

The figure 5, which follows the pattern of figure 4, illustrates this effect. We consider for values of  $k = 2, 1.5, 1, 0.5$  and  $0$ .  $k = 2$  is the perturbative effect

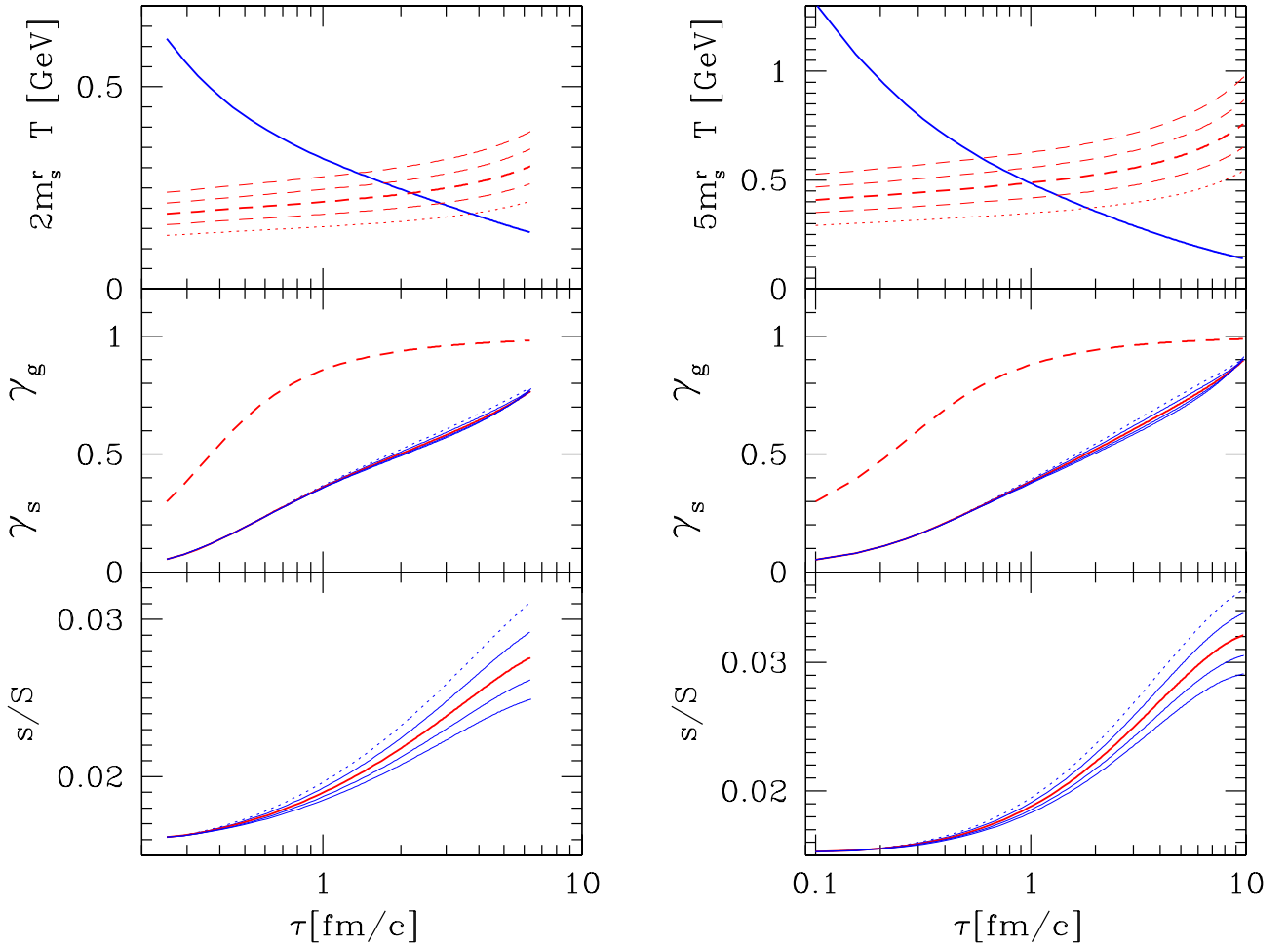


FIG. 6: (color online) Study of  $s/S$  evolution with  $\tau$  in dependence on strange quark mass, dashed and dotted lines, top panels. Left for RHIC, right for LHC, V1 expansion model. Figure structure same as figure 4 and 5. Top panel shows the range of masses  $m_s^r$  we consider with the middle line being our standard reference value and dotted lines being the corresponding cases.

seen for massless quarks,  $k = 0$  corresponds to no effect of interaction, when  $m_s \gg T$ . When  $k = 0$ , the strange quark degeneracy is largest, thus for a given strangeness yield  $s$  the value of  $\gamma_s$  is smallest. and the production of strangeness biggest. Consequently, this value corresponds to the smallest  $\gamma_s$  in the middle panels of figure 5 and greatest value of  $s/S$  in the bottom panels. Other lines follow and the middle (red on line lines) correspond to  $k = 1$  we used to obtain the reference results presented earlier.

A similar effect arises considering variation of strange quark mass as shown by dashed lines in top panels of figure 6. We vary by factor 2 the strange quark mass as is seen in the top panel of the figure 6, on left for RHIC and on right for LHC. The way this effect plays out we can understand considering that when the strange quark mass is increased, the equilibrium strangeness density is decreased, and thus, for a given strangeness yield  $s/S$ , the value of  $\gamma_s$  is increased, which in turn reduces strangeness production strength. Smallest mass considered (dotted line in top panels of figure 6) corresponds

to the largest final value of  $s/S$  shown by dotted line in the bottom panels. What is more surprising is that the effect of mass variation *cancels* in the actual computed  $\gamma_s$  shown in the middle panels. The reason for this accidental cancellation is that for a larger mass the smaller value of final  $s/S$  solves for the same value of  $\gamma_s$ , see Eq. (10).

Since both  $m_s$  and the interaction effect on the strange quark density is today not understood at sufficiently precise level, the appearance of a possible range of values at freeze-out, for both  $\gamma_s$  and  $s/S$  in figures 5 and 6 signals (correlated) uncertainty in the understanding of the results at RHIC and predictive power for LHC.

#### IV. CONSEQUENCES FOR HADRON YIELDS AND THEIR CHANGES FROM RHIC TO LHC

##### A. Strangeness and entropy

The value of  $dS/dy = 20,000$  (4 times RHIC) at LHC is no more than an educated guess, thus we first ex-

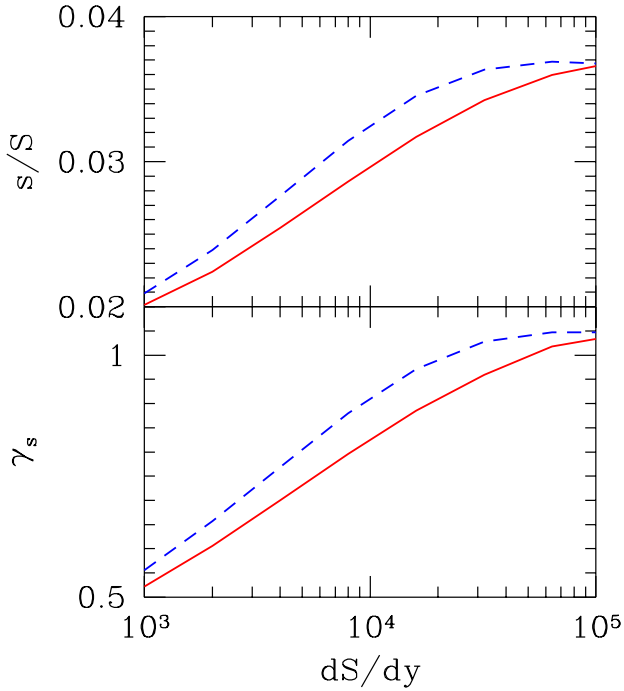


FIG. 7: (color online) Summary of the results for  $s/S$  (top panel) and  $\gamma_s$  (bottom panel) for the most central 5% collisions as function of reaction  $dS/dy$  — the values  $dS/dy = 5,000$  and  $dS/dy = 20,000$  had served as reference points for RHIC and LHC, respectively. The bulk transverse expansion model V1 is the solid line, the dashed line is the donut expansion model V2 with  $d = 3.5$  fm.

plore a range of  $dS/dy$  input values. In figure 7, we present a more systematic exploration of the freeze-out strangeness observables as function of  $dS/dy$  in a range which span the domain from the SPS energy range to the most hadron rich hypothesis about LHC. We see a gradual rise of both  $s/S$  and  $\gamma_s$  as function of  $dS/dy$  which begins to saturate for  $dS/dy > 20,000$ . These results are for the most central 5% reactions, the solid lines are for V1 homogeneous expansion and dashed lines for V2 donut expansion model.

We expect that  $dS/dy \propto dh/dy$ , thus the result seen in figure 7 implies that the specific yield and occupancy of strangeness rises nearly linearly with  $dh/dy$ . To quantify this observation, we present, in figure 8, how the yield of charged hadrons relates the entropy yield. These results were obtained both for RHIC (left region, red on line) and LHC (right region) by the methods described in Ref. [32]. The difference between RHIC and LHC is that we take the thermal energy per baryon at RHIC to be  $E/b = 40$  GeV and following Ref. [32]  $E/b = 412$  GeV at LHC. However, this limits the range of possible entropy yield to just below the value we studied in this paper. A slight increase in assumed  $E/b$  would recenter the LHC results seen in figure 8 at  $dS/dy = 20,000$ , four times the RHIC range, which we use in this paper.

The choice of energy per baryon content,  $E/b$ , in the

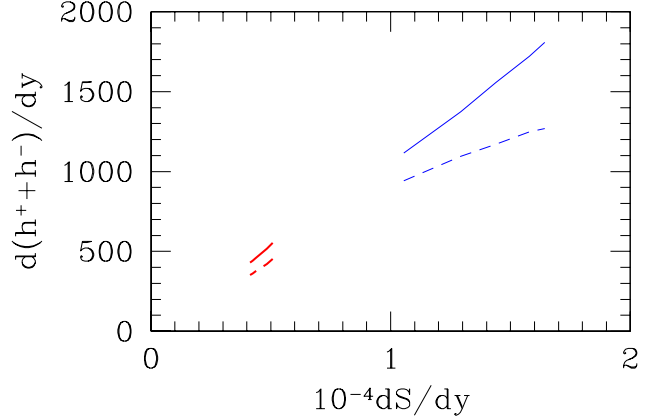


FIG. 8: (color online) The yield of charged hadrons  $d(h^- + h^+)/dy$  for different values of  $dS/dy$ , left domain for RHIC and right domain for LHC. Solid lines: after all weak decays, dashed lines: before weak decays.

hadronizing fireball is the sole change we need to implement to change the physics environment from RHIC to LHC and to obtain other parameters of relevance. These parameters are implicitly fixed by constraints such as equations of state, strangeness conservation, participant number. As a result, we find the expected shift down from RHIC to LHC in chemical potentials, and a subtle change in freeze-out temperature: while at RHIC, in full chemical non-equilibrium, the method of Ref. [32] produces  $T = 0.14$  GeV, at LHC the value drops to  $T = 0.125$  GeV, consistent with the greater expected supercooling of more explosive fireball expansion and chemical non-equilibrium QGP freeze-out. In figure 8, we present yields accounting for weak strangeness decays (solid lines), and prior to weak decays (dashed lines). Charm decay into hadrons at LHC was not considered, and may contribute ‘visibly’.

The specific strangeness per entropy content,  $s/S$  is determining the relative yield of strange to non-strange particle yields. We show this in figure 9, where thick lines with  $s/S < 0.3$  are for RHIC, and LHC (thin lines) environments. Solid lines are before weak decays and dashed after weak decays, which dilute the pion yield. RHIC and LHC lines sometimes overlap, indicating partial cancellation and/or negligible influence of the chemical potential and temperature shift effects. See, for example, the important case of the  $K^+/\pi^+$ -ratio, bottom panel.

The top three panels, in figure 9, indicate that the multistrange particle yields change rather rapidly. The thermal production of strangeness which increases  $s/S$  by  $40 \pm 10\%$  from the value expected in  $pp$  reactions, increases the ratios  $\phi(\bar{s}s)/\pi^+$ ,  $\Xi^-(ssd)/\pi^+$  by factor about 5, and the ratio  $\Omega^-(sss)/\pi^+$  by factor 15. The ratio of  $K^+/\pi^+$  is shown in bottom of figure 9, and it varies by about factor 2–3, which is quite significant and of interest as values as large as  $K^+/\pi^+ \simeq 0.25$  possible in most central LHC reactions have never been seen before. An

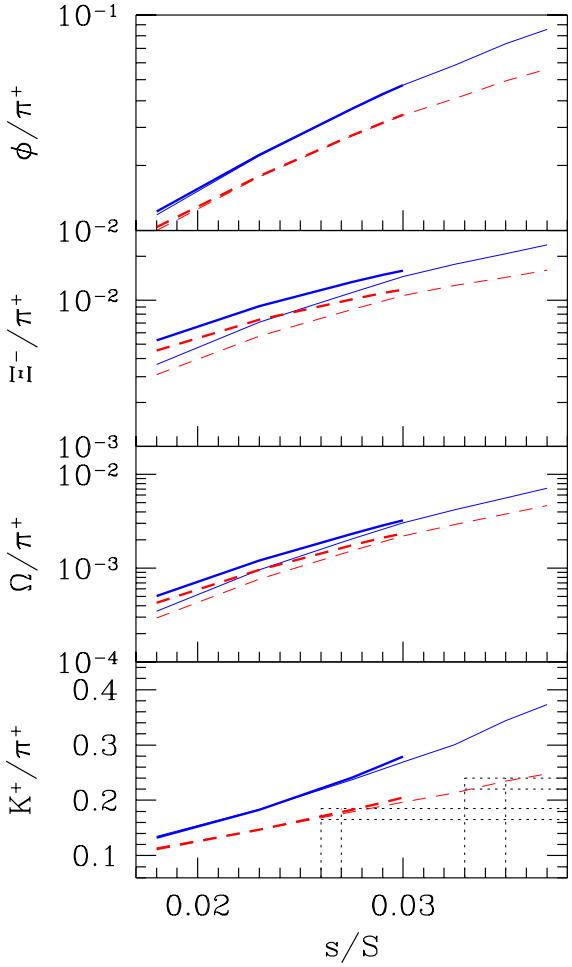


FIG. 9: (color online) Relative particle yields as function of  $s/S$ , the attained specific strangeness per entropy at QGP freeze-out. From top to bottom, multistrange particle yields per pion  $\Phi/\pi^+$ ,  $\Xi^-/\pi^+$ ,  $\Omega^-/\pi^+$  (log scale) followed by  $K^+/\pi^+$  ratio at bottom. Solid lines primary relative yields, dashed lines after all weak decays. Thick line with  $s/S < 0.3$  are for RHIC and thin lines are for LHC physics environment.

increase by about 40% is predicted from  $K^+/\pi^+ = 0.17$  at RHIC to  $K^+/\pi^+ = 0.25$  at LHC as indicated by dotted lines guiding the eye, corresponding to the expected increase of  $s/S$ .

## B. Thermal charm at RHIC and LHC

The direct initial high energy parton collisions dominate production of the massive flavor, charm and bottom, and a thermal process seems to be of no interest. However, there are two questions we can investigate:

- considering that  $\gamma_c$  in the deconfined phase can be as large as  $\gamma_c \simeq 100$  is there any significant thermal annihilation of charm in the QGP evolution?
- how large is the thermally produced charm yield and can it lead to chemical equilibrium of charmed quarks?

The interest in question a) needs no further discussion. Question b) is of interest since the directly produced charmed quarks are in principle not easily thermalized, while the thermally produced charmed quarks emerge naturally in a momentum distribution imaging their ‘parent’ particles thermal momentum distribution. Consequently, the thermally produced charmed quarks provide a solid thermal lower limit for the yield of charm, with the directly produced charm contributing to thermal distribution after charm has been subject to collisions required for thermalization.

We see the results of this study in figure 10, on left for RHIC, on right for LHC. The top panels as usual presents the temperature and here, charmed quark mass, scaled with factor 1/10 at RHIC and 1/2 at LHC (on right). The middle panel presents (dotted line)  $\gamma_g$ , (solid line) the charm phase space occupancy,  $\gamma_c$  and (dashed line)  $\gamma_c$  obtained solely by *thermal processes*. Similarly, in the bottom panels, the dashed lines are the thermal yield at RHIC and LHC, while the horizontal lines are the (little) evolving  $c/S$  yields including the directly produced charm. The direct charm production at RHIC is expected to be 500 times greater than the thermal process. At LHC, the higher initial temperature but unchanged specific direct yield  $c/S$  in parton collisions, suggests that thermal production is just factor 30 times smaller. However, this factor depends on good understanding of both processes and the initial conditions and surely cannot be fully trusted. Moreover, there is the possibility that the directly produced charm at LHC may not well thermalized, in which case an appreciable fraction of thermal charm yield could indeed originate in thermal reactions.

The answers to the opening questions thus are:

- there is no visible charm reannihilation, as we see in the bottom panel, see the nearly horizontal lines at  $c/S = 10^{-3}$ ; note that the direct charm yield, we assumed implicitly, is obtained by multiplying the  $c/S \simeq 10^{-3}$  yields with  $dS/dy = 5,000$  on left for RHIC, yielding  $dc/dy|_{\text{RHIC}} = 15$ , and with  $dS/dy = 20,000$  on right for LHC, yielding  $dc/dy|_{\text{LHC}} = 60$ .
- in the middle panel, we see that thermal production alone (dashed lines) oversaturates the charm phase space, the thermal produced charm phase space occupancy  $\gamma_c^{\text{th}}$  (dashed lines middle panels) cross the gluon dotted  $\gamma_g$  line at around  $4.7 \text{ fm}/c$  for RHIC (corresponding to  $T \simeq 0.19 \text{ GeV}$ ) and at  $6 \text{ fm}/c$  (corresponding to  $T \simeq 0.20 \text{ GeV}$ ) at LHC.

## V. SUMMARY AND CONCLUSIONS

We have studied, in detail, the thermal QGP based strangeness production at RHIC and LHC, and have interpreted the observed final  $s$ -yield in terms of our theoretical knowledge about the properties of the QGP phase. Our aim has been to understand how the overall final state strange quark flavor has been produced, and to study in detail the mechanisms behind strangeness en-

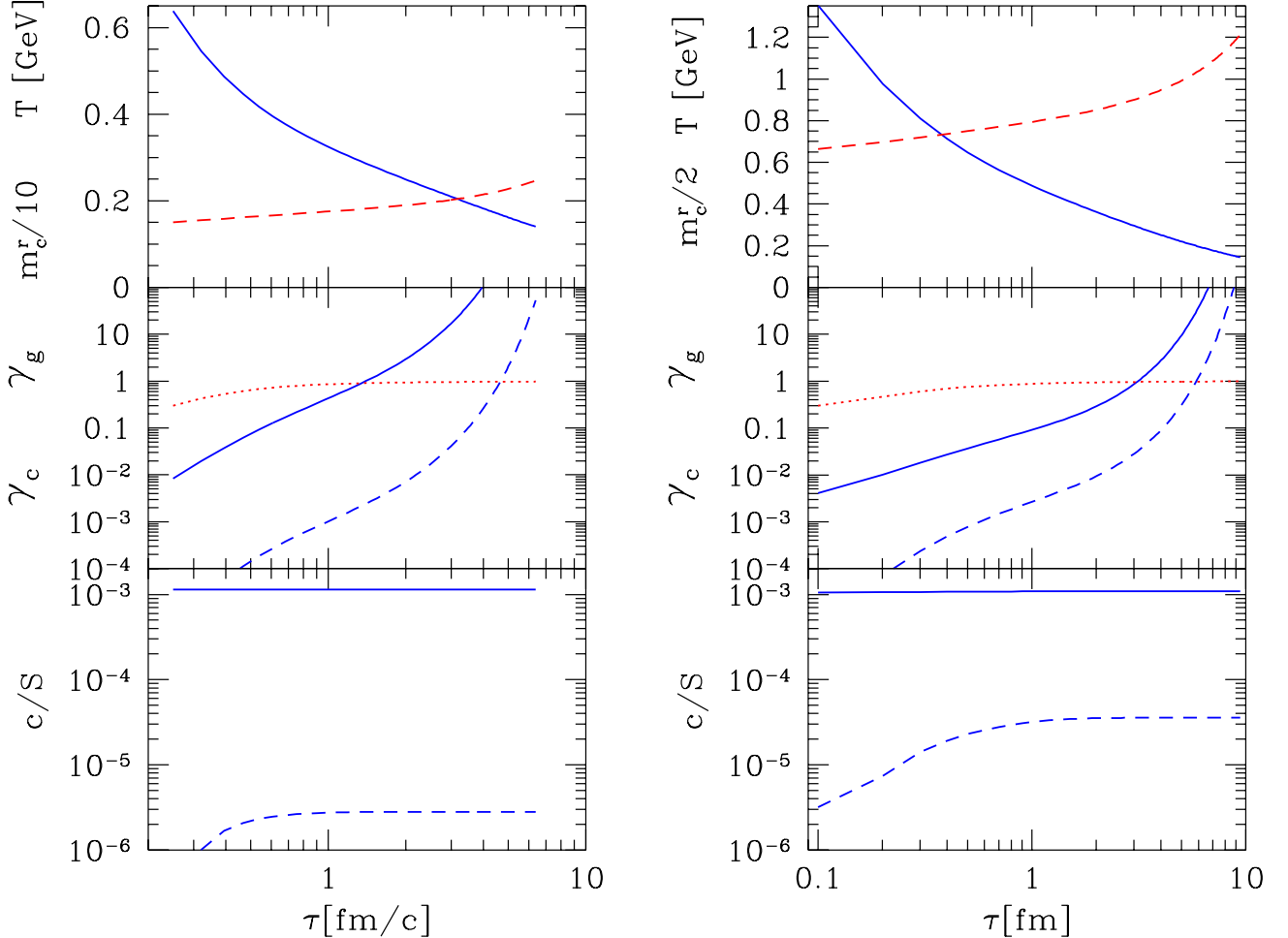


FIG. 10: (color online) Left RHIC and right LHC for charm production. Figure structure same as figures 2–6. Top panel: solid lines  $T$ , dashed lines, running  $m_c^r$ , scaled with 10 for RHIC on left and with 2 on right for LHC; middle panel: dotted line  $\gamma_g$ , solid lines the computed total charm  $\gamma_c$ , dashed lines  $\gamma_c$  corresponding to thermal charm production; and bottom panel: specific charm yield per entropy, solid lines for all charm, and dashed lines for thermally produced charm.

hancement. Our results suggest that strangeness enhancement could be studied considering:

$$R_{\text{CP}}^s \equiv \frac{s/S|_{\text{central}}}{s/S|_{\text{peripheral}}} = \frac{s/S(\tau_f)}{s/S(\tau_0)}. \quad (25)$$

The central strangeness yields is just the final value we find at freeze-out, while the peripheral yield is the initial value before thermal strangeness production begins. Our study shows that  $R_{\text{CP}}^s \in 1.6, 2.2$ , with the precise result depending on details such as strange quark mass, see figure 6, reaction energy, dynamics of expansion, see figure 1.

More generally, one can envisage to use  $d(h^+ + h^-)/dy$  as a measure of entropy content, see figure 8. Also, instead of the total strangeness one may consider enhancement of individual (multi)strange particles. We note here that the overall gradual enhancement of the strangeness yield with centrality, at the level a factor 1.6–2.2 is accompanied by a drastically greater enhancement of multi strange hadron yields, shown in figure 9.

Aside of centrality dependence, we have also explored within the framework of our model an extrapolation from RHIC to LHC physics environments. More generally, we have presented in figure 7 the reaction energy dependence by considering the  $s/S|_{\text{central}}$  yields as function of  $dS/dy$ .

One of the interesting results obtained, is the approach to chemical strangeness equilibrium in the deconfined QGP phase formed in most central and high energetic RHIC reactions. The evidence for this is implicit in the experimentally reported yields of strange hadrons, which lead to values of specific strangeness per entropy at the level of  $s/S \simeq 0.028$  [21]. Given the near chemical equilibration at RHIC, and within the models considered even possibly a slight over saturation at LHC, for the most central 5% reactions there is no relevant dependence of strangeness production on initial conditions established in the reaction. We have demonstrated this in a picture-book fashion, see figure 4, where, for a wide range of initial conditions, the same final strangeness yield and

equilibrium condition arises after  $\Delta\tau = 2\text{--}3 \text{ fm}/c$  evolution.

On the other hand, the more peripheral reactions do not saturate the phase space, in that both  $\gamma_s^{\text{QGP}} < 1$ , and  $s/S < 0.03$ . Thus the peripheral yields should be more sensitive to the initial conditions, and thus are also somewhat dependent on model assumptions about initial state and evolution dynamics. We have shown, in figures 2 and 3, the impact parameter dependence that arises in our two favorite volume expansion models, without making an effort to compare this to the experimental results. However, it is quite clear that there is good qualitative agreement with the analysis results presented in Ref. [21]. Similarly, the gradual rise of strangeness yield  $s/S$  with  $dS/dy$ , seen in figure 7, is nearly exactly reminiscent of the rise with reaction energy obtained in a analysis of particle yields obtained at different reaction energies [28].

We have made a (conservative) prediction regarding the increase in the  $K^+/\pi^+$  ratio at LHC compared to RHIC, see figure 9. A greater increase is possible, depending on both:

- 1) the dynamics of the volume expansion — this can enhance the strangeness oversaturation of the final QGP state, see figures 2 and 3, and
- 2) QCD details, such as strange quark density including QCD interactions, and (still not well understood) strange quark mass, see figures 5 and 6.

Since chemical equilibration of strangeness, in QGP formed in the 5% most central top RHIC energy reactions, cannot be disputed, we also have now a better understanding of the resulting oversaturation of the hadron phase space by strangeness. The magnitude of this effect, dependent on the temperature of hadronization, can be considerable. This can be easily seen considering the magnitude of  $s/S$  in both QGP and HG phases. The

final state hadrons formed far-off chemical equilibrium cannot significantly adjust chemical composition, considering the rapid breakup of the fireball, during the period of about 1–2 fm/ $c$  prior to onset of the free flow. Thus our finding is that strangeness rich QGP enhances decisively the yields of multistrange hadrons. This phenomenon is more accentuated considering charmed hadrons containing strangeness, a topic under current investigation.

Furthermore, using the methods developed here, we have considered thermal charm production. At LHC, we find a nearly physically relevant thermal charm production, but not at RHIC. However, the thermal process we consider is able to produce enough charm to oversaturate the final state at both RHIC and LHC, see figure 10. This also shows that the direct parton collision based production at RHIC leads to extraordinarily large values of  $\gamma_c$ . The chemical nonequilibrium of charm is thus more pronounced than that of strangeness.

**In conclusion:** The totality of our results shows that, as function of entropy yield (energy of A–A reaction) and geometric reaction size (impact parameter dependence), the phenomenon of strangeness enhancement is well described by the mechanism of thermal (gluon fusion) strangeness production in QGP. We find both, as function of centrality, and energy, a gradual increase in specific strangeness yield, which agrees with all available experimental results.

#### Acknowledgments

Work supported by a grant from: the U.S. Department of Energy DE-FG02-04ER4131. LPTHE, Univ. Paris 6 et 7 is: Unité mixte de Recherche du CNRS, UMR7589.

---

[1] B. B. Back *et al.*, Nucl. Phys. A **757**, 28 (2005) [arXiv:nucl-ex/0410022].  
[2] J. Rafelski and B. Müller, Phys. Rev. Lett. **48**, 1066 (1982) [Erratum-ibid. **56**, 2334 (1986)].  
[3] J. Letessier, A. Tounsi and J. Rafelski, Phys. Lett. B **389** (1996) 586.  
[4] P. Koch and J. Rafelski, Nucl. Phys. A **444**, 678 (1985).  
[5] P. Koch, B. Muller and J. Rafelski, Phys. Rept. **142**, 167 (1986).  
[6] P. Koch, J. Rafelski and W. Greiner, Phys. Lett. B **123**, 151 (1983).  
[7] P. Braun-Munzinger, K. Redlich and J. Stachel, arXiv:nucl-th/0304013.  
[8] J. Rafelski and M. Danos, Phys. Lett. B **97**, 279 (1980); J. Rafelski and J. Letessier, J. Phys. G **28**, 1819 (2002) [arXiv:hep-ph/0112151].  
[9] S. Hamieh, K. Redlich and A. Tounsi, Phys. Lett. B **486**, 61 (2000) [arXiv:hep-ph/0006024].  
[10] K. Redlich and A. Tounsi, Eur. Phys. J. C **24**, 589 (2002) [arXiv:hep-ph/0111261].  
[11] K. Geiger, Phys. Rev. D **46**, 4965 (1992).  
[12] L. Xiong and E. V. Shuryak, Phys. Rev. C **49**, 2203 (1994) [arXiv:hep-ph/9309333].  
[13] Z. Xu and C. Greiner, Phys. Rev. C **71**, 064901 (2005) [arXiv:hep-ph/0406278].  
[14] J. Rafelski and J. Letessier, Nucl. Phys. A **702**, 304 (2002) [arXiv:hep-ph/0112027].  
[15] P. Koch, B. Muller and J. Rafelski, Z. Phys. A **324**, 453 (1986).  
[16] T. Matsui, B. Svetitsky and L. D. McLerran, Phys. Rev. D **34**, 783 and 2047 (1986) [Erratum-ibid. D **37**, 844 (1988)].  
[17] T. S. Biro, E. van Doorn, B. Müller, M. H. Thoma and X. N. Wang, Phys. Rev. C **48**, 1275 (1993) [arXiv:nucl-th/9303004].  
[18] D. Pal, A. Sen, M. G. Mustafa and D. K. Srivastava, Phys. Rev. C **65**, 034901 (2002) [arXiv:nucl-th/0105032].  
[19] Z. J. He, J. L. Long, Y. G. Ma, G. L. Ma and B. Liu, Phys. Rev. C **69**, 034906 (2004).  
[20] H. T. Elze, J. Rafelski and L. Turko, Phys. Lett. B **506**,

123 (2001) [arXiv:hep-ph/0103066].

[21] J. Rafelski, J. Letessier and G. Torrieri, Phys. Rev. C **72**, 024905 (2005), [arXiv:nucl-th/0412072].

[22] T. Sjostrand, L. Lonnblad, S. Mrenna and P. Skands, “PYTHIA 6.3: Physics and manual,” arXiv:hep-ph/0308153, see in particular section 12 p337ff.

[23] M. Bedjidian *et al.*, “Hard probes in heavy ion collisions at the LHC: Heavy flavour physics,” chapter 3 in CERN-Yellow report 2004-009, Proceedings of the CERN workshop *Hard Probes in Heavy Ion Collisions at the LHC*, see <http://cdsweb.cern.ch/search.py?recid=815037&ln=en>, arXiv:hep-ph/0311048.

[24] S. Mrowczynski, arXiv:hep-ph/0511052, and references therein.

[25] J. Letessier and J. Rafelski, Phys. Rev. C **67**, 031902 (2003) [arXiv:hep-ph/0301099].

[26] J. Letessier, J. Rafelski and A. Tounsi, Phys. Rev. C **50**, 406 (1994) [arXiv:hep-ph/9711346].

[27] T. S. Biro, P. Levai and B. Muller, Phys. Rev. D **42** (1990) 3078.

[28] J. Letessier and J. Rafelski, “Hadron production and phase changes in relativistic heavy ion collisions”, arXiv:nucl-th/0504028.

[29] J. Letessier and J. Rafelski, “Hadrons and quark - gluon plasma”, Cambridge Monogr. Part. Phys. Nucl. Phys. Cosmol. **18**, 1 (2002).

[30] J. Rafelski and J. Letessier, Phys. Lett. B **469**, 12 (1999).

[31] S. A. Chin and A. K. Kerman, Phys. Rev. Lett. **43**, 1292 (1979).

[32] J. Rafelski and J. Letessier, Eur. Phys. J. C **45**, 61 (2006) [arXiv:hep-ph/0506140].